Structural Changes in Bacteriorhodopsin During Ion Transport at 2 Angstrom Resolution

Hartmut Luecke,[1,2,3]* Brigitte Schobert,[2,3] Hans-Thomas Richter,[2,3] Jean-Philippe Cartailler,[1,3] Janos K. Lanyi[2,3]*

Crystal structures of the Asp[96] to Asn mutant of the light-driven proton pump bacteriorhodopsin and its M photointermediate produced by illumination at ambient temperature have been determined to 1.8 and 2.0 angstroms resolution, respectively. The trapped photoproduct corresponds to the late M state in the transport cycle—that is, after proton transfer to Asp[85] and release of a proton to the extracellular membrane surface, but before reprotonation of the deprotonated retinal Schiff base. Its density map describes displacements of side chains near the retinal induced by its photoisomerization to 13-*cis*,15-*anti* and an extensive rearrangement of the three-dimensional network of hydrogen-bonded residues and bound water that accounts for the changed pK_a values (where K_a is the acid constant) of the Schiff base and Asp[85]. The structural changes detected suggest the means for conserving energy at the active site and for ensuring the directionality of proton translocation.

Active transport of ions against their electrochemical potentials across cell and organelle membranes is carried out by proteins that couple an energy-yielding reaction, such as hydrolysis of adenosine triphosphate, electron transfer, or isomerization of retinal, to the transmembrane movement of ions. The mechanism of this kind of transport is a major, still unsolved, problem of membrane bioenergetics. A satisfactory mechanism will explain how the free energy gain from the driving reaction is used to change, in an ordered way, the affinities of binding site(s) for the transported ion and how the alternating accessibility of these ion binding site(s) to the two membrane surfaces is mediated. Crystallographic structures are available for only a few transport proteins, and much effort is expended to improve their resolutions to give unambiguous answers to these questions.

Bacteriorhodopsin is a light-driven proton pump, energized by the all-*trans* to 13-*cis* photoisomerization of the retinal chromophore (*1*). This small (26 kD) protein consists of seven transmembrane helices, A through G, and short extramembrane segments (*2–5*). The structure of the unphotolyzed (BR) state, determined most recently at 1.55 Å resolution (*6*), revealed a three-dimensional interconnected hydrogen-bonded network of protein residues and water molecules between the centrally located protonated retinal Schiff base and the extracellular surface and provided clues about how release of a proton to the extracellular membrane surface might be coupled to deprotonation of the Schiff base. The local π-bulge distortion of helix G, with hydrogen bonding of two main-chain C=O groups to water molecules (*6*), suggested, in turn, that translocation of a proton from the cytoplasmic surface to the Schiff base might be linked to the shift of the protein conformation evident from low-resolution difference maps (*7, 8*). Understanding how these processes cause the unidirectional translocation of a proton requires description of the structural changes in the J, K, L, M, N, and O intermediates (*9*) of the transport cycle. The overall structure of the protein and the sequence of proton transfers that add up to the full translocation of a proton from one side of the membrane to the other are shown in Fig. 1. The crucial intermediate is the M state, because in M the Schiff base is deprotonated, Asp[85] to its extracellular side is protonated, and a proton has been released to the surface, but Asp[96] to its cytoplasmic side has not yet become deprotonated—that is, this state is after step 2 but before step 3 in Fig. 1.

From spectroscopic and kinetic measurements of wild-type and mutant bacteriorhodopsins, several substates of the M intermediate have been identified and distinguished by their accessibilities to the two membrane surfaces. In the early M state or states, the proton connectivity of the Schiff base is to the extracellular side, whereas in the late M state(s) it is to the cytoplasmic side (*10, 11*). Transition of M_1 to M_2 (*12*) is associated with proton release to the extracellular surface (*10, 13*). Under physiological conditions, the pH is well above the pK_a (where K_a is the acid constant) for proton release, making the M_1 to M_2 reaction unidirectional and shifting the protonation equilibrium between Asp[85] and the Schiff base in the kinetic scheme ($L \leftrightarrow M_1$) fully toward deprotonation of the Schiff base (that is, $L \leftrightarrow M_1 \rightarrow M_2$).

There is some uncertainty about the timing and the nature of structural changes in the photocycle. From low-resolution difference maps in projection, it is evident that large-scale changes of helices F and G at the cytoplasmic surface occur in the late M state (*7, 14*). In contrast, large changes of amide I bands in Fourier transform infrared spectroscopy (FTIR) difference spectra (*15*), and displacement of helix F as measured by spin-spin coupling of labels on cytoplasmic interhelical loops (*16*), are seen only in the N state. In the Asp[96] to Asn (D96N) mutant, reprotonation of the Schiff base is greatly slowed, and the late M state

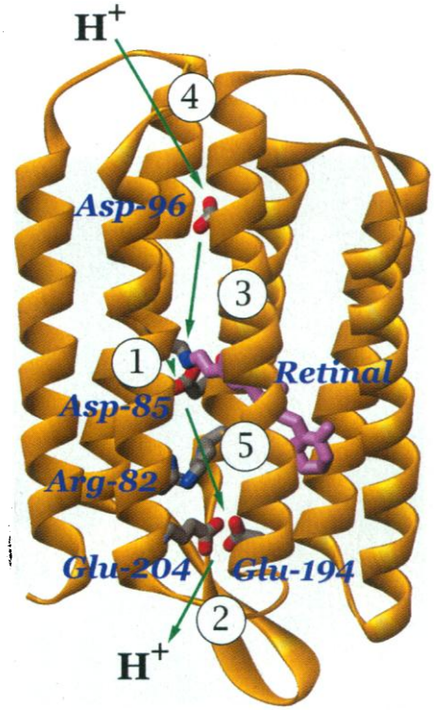

Fig. 1. Overall view of bacteriorhodopsin, shown with the retinal (purple) and residues directly implicated in proton transport. Top, Cytoplasmic side. Arrows indicate proton transfer steps during the photochemical cycle. Numbers refer to the sequential order: (1) deprotonation of the Schiff base, protonation of Asp[85]; (2) proton release to the extracellular surface; (3) reprotonation of the Schiff base, deprotonation of Asp[96]; (4) reprotonation of Asp[96] from the cytoplasmic surface; and (5) deprotonation of Asp[85], reprotonation of the proton release site. Coordinates are from (*6*).

[1]Department of Molecular Biology and Biochemistry, [2]Department of Physiology and Biophysics, [3]UCI Program in Macromolecular Structure, University of California, Irvine, CA 92697, USA.

*To whom correspondence should be addressed. E-mail: hudel@uci.edu or jlanyi@orion.oac.uci.edu

(termed M_N) contains the changed amide I bands of N (*17*). Although M_N might have some features unique to the D96N mutant (*18*), at 3 Å resolution and in projection its structure is indistinguishable from M of the wild-type protein (*14*). The M_N state of D96N is easier to trap in a photostationary state than M of the wild type because the much slower decay allows virtually full conversion of the BR state to M_N. For this reason, we grew crystals of the D96N mutant in the cubic lipid phase (*19*), converted them to the M_N state by illuminating with yellow light at 290 K, and determined the structural changes after rapid cooling to 100 K.

Structure of the D96N Mutant in the BR State

Data and refinement statistics for the BR state of D96N are shown in Table 1. Virtually no differences between the light-adapted forms of the D96N mutant and the wild-type protein are detected except at the location of the residue change. The hydrogen bond between the carboxyl oxygen of the protonated Asp^{96} and the hydroxyl of Thr^{46} in the wild type is replaced by a new water, 504, that bridges ND-2 of Asn^{96} and OG-1 of Thr^{46}. Another well-defined water, 503, whose presence is ambiguous in the wild type, connects water 501 to OG-1 of Thr^{178}. A structural role for residue 96 in the unphotolyzed state, implied by these results, is not evident from electron diffraction of D96N at 3 Å resolution (*14*) but was anticipated from a structural difference between the D85N and D85N–D96N mutants (*20*).

M State: Structural Changes in the Retinal

Data and refinement statistics for the M state of the D96N mutant are shown in Table 1. Because of local disorder at the cytoplasmic ends of helices F and G, the quality of electron-density maps and the crystallographic R factors of this photocycle intermediate are inferior to those of the BR state. We report here only features that are common to four independently collected and refined M state structures.

According to overwhelming evidence from resonance Raman and nuclear magnetic resonance spectra, the configuration of the retinal in the M state(s) is 13-*cis*,15-*anti*. The disposition of the polyene chain and its changes in M as well as its angle to the membrane plane and its changes have been estimated from transient linear dichroism in the visible and the infrared (*21*) during the photocycle. Earnest *et al.* (*21*) reported the angles between the conjugated π system of the retinal and the bilayer plane in the BR and M states to be 21° and 28°, respectively. The positions of the ring and the 13-methyl group in the unphotolyzed state have been determined by neutron diffraction of protein with specifically deuterated retinals (*22*). In M the retinal indeed assumes the 13-*cis*,15-*anti* configuration (Fig. 2). The kinking of the *cis*-retinal moves the polyene chain between C-10 and the Schiff base nitrogen toward the cytoplasmic side. The largest relative movement is for C-14, which is displaced by 1.7 Å. The 13-methyl group moves by 1.3 Å toward the cytoplasmic side. In comparison, the movement of the β-ionone ring by 0.4 Å toward the Schiff base is relatively minor. The measured angles between the conjugated π system of the retinal and bilayer plane for the BR and M states are 20.2° and 29.6°, respectively, which is in excellent agreement with the polarized infrared results (*21*).

Structural Changes at the Retinal Binding Site, at the Schiff Base, and in the Extracellular Region

The side chains of several residues in the retinal binding pocket are rearranged in the M state (Fig. 2). The main chain and the side chain of Lys^{216} move, with the α carbon accommodating the *cis*-retinal kink by a 1 Å motion in the extracellular direction. The side chain of Trp^{182} is displaced by 1.5 Å in the cytoplasmic direction because of its proximity to the 13-methyl group, and the side chain of Leu^{93}, also near the 13-methyl group, is rotated by about 90° (χ_1 by −26°, χ_2 by −65°). Trp^{86}, on the extracellular side of the retinal, tilts toward the polyene chain that has moved away from it. Residues that contact the β-ionone ring (Trp^{138}, Ser^{141}, and Met^{145}) are moved much less, consistent with its lesser displacement. It appears, therefore, that the steric conflict that develops upon rotation of the C-13=C-14 double bond between the retinal chain and the protein involves primarily the 13-methyl group and the side chains of three residues that make contact with it and with the retinal chain. The slowing of thermal reisomerization of the retinal during the photocycle in mutants of Leu^{93} (*23*) as well as in W182F (*24*) had suggested such an interaction. CE of Met^{118}, which is close (3.6 Å) to the 9-methyl group in BR, is moved by 2.1 Å, but this is probably not a direct response to the isomerization because the 9-methyl group is displaced by <0.3 Å. Similarly, the rotation of the ring of Phe^{219} in Fig. 2 is an indirect response to movement of the retinal.

As shown in Figs. 3 and 4, the active site undergoes considerable rearrangement. In the unphotolyzed state, water 402 accepts a hydrogen bond from the protonated retinal Schiff base and donates hydrogen bonds to the anionic Asp^{85} and Asp^{212} (*4, 6*). This complex forms the center of a network that stabilizes the separated charges in this buried region. Asp^{85} is hydrogen-bonded to the side chain of Thr^{89}. Water 401 is hydrogen-bonded to Asp^{85} on the one hand and through water 406 to Arg^{82} on the other. Asp^{212} in

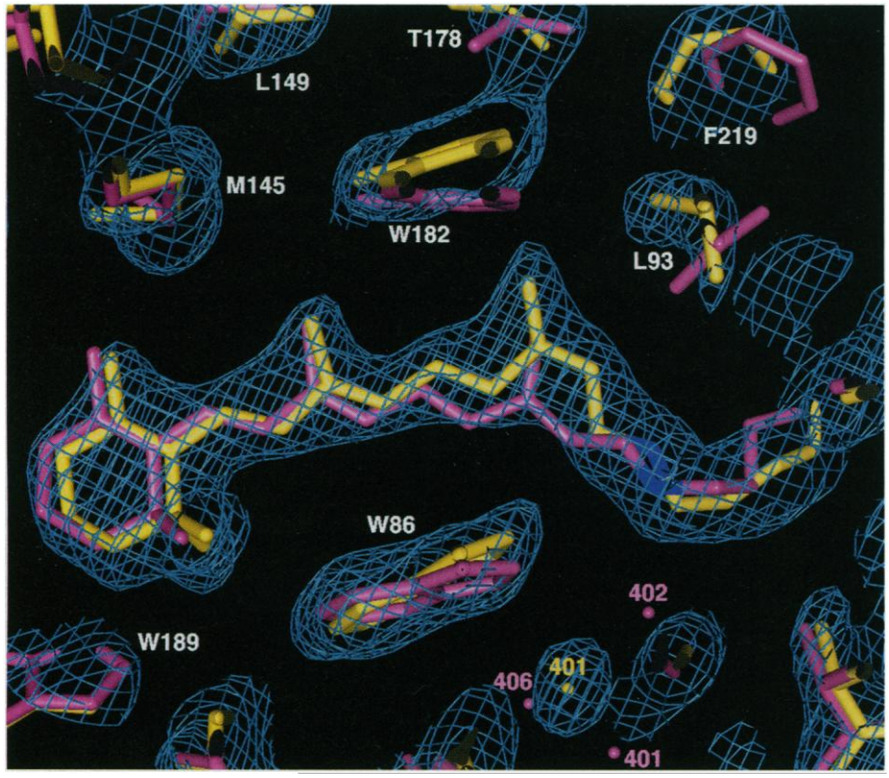

Fig. 2. View of retinal and the surrounding region (*37*). The $2F_o-F_c$ electron density map of the M state contoured at 1σ is shown in blue. The corresponding M state atomic model is shown in yellow. Also shown, for reference, is the atomic model of the BR (ground) state in purple. The cytoplasmic half of the ion pump is above the retinal, and the extracellular half is below the retinal.

turn is hydrogen-bonded to Tyr^{185} and Tyr^{57}. In the M state, the retinylidene nitrogen is moved toward the cytoplasmic side by 0.9 Å and its electron pair is turned away from Asp^{85}. The OD-1 of Asp^{85} is now 1.2 Å farther away from the Schiff base nitrogen. Either because of the isomerization of the retinal, or because of the proton transfer that follows it, water molecules 401, 402, and 406 are replaced by a single water, 401, that is moved from its position in the BR state by 1.9 Å and that now occupies the center of gravity of the former three water molecules (Fig. 3). The protonated Asp^{85} has lost all its former hydrogen-bonding partners, except water 401, whereas Asp^{212} retains its connection to the phenolic OH groups of Tyr^{185} and Tyr^{57} and forms a new hydrogen bond to water 401 and to the previously unsatisfied indole nitrogen of Trp^{86}.

In M_N, the measured pK_a of the Schiff base is greatly lowered (*25*), and it has been assumed that this is largely because the retinylidene nitrogen is displaced into a highly hydrophobic region by isomerization of the retinal, as we now find. In the new environment of the Schiff base, the geometry for a hydrogen bond with water 402 that is polarized by Asp^{85} and Asp^{212} in the BR state is unfavorable. Instead, the Schiff base faces toward Leu^{93} and Val^{49}. Likewise, there are drastic changes around Asp^{85} that account for the proposed (*26, 27*) greatly increased pK_a of this residue. Two of the three previous hydrogen bonds are lost and, in the third bond, to water 401, the carboxyl oxygen of Asp^{85} could now be the proton donor, further stabilizing its protonated state. The structure near Asp^{85} (Fig. 3) is consistent with dehydration as the cause of the high frequency of the protonated carboxyl stretch of this residue (*27*).

Toward the extracellular side, a three-dimensional network of hydrogen-bonded side chains and water connects the active site of the BR state with the residues that participate in the release of a proton to the extracellular surface upon protonation of Asp^{85}—that is, Arg^{82}, Glu^{194}, and Glu^{204} (shown schematically in Fig. 4A). One continuous chain is through water 406, which connects both Asp^{85} (through waters 401 and 406) and Asp^{212} (through water 406) to the NH-1 of Arg^{82} (*6*). This chain is disconnected in M, because water 406 is absent (Fig. 4B). The second chain, from Asp^{85} to both NH-1 and NH-2 of Arg^{82}, in the unphotolyzed state is through water 402, Asp^{212}, Tyr^{57}, and water 407 (*6*). This chain is retained, but, because the side chain of Arg^{82} moves downward (CZ is displaced by 1.6 Å along the *z* axis), it connects only to NH-1.

In the BR state, NH-1 and NE of Arg^{82} are both connected to Glu^{194}, through water molecules 403 and 404, whereas the side-chain oxygens of Glu^{194} and Glu^{204} are connected directly through a hydrogen bond (*3, 6*). In M, Glu^{194} retains its connection only with the NE of Arg^{82}. The connection between Glu^{194} and Glu^{204} is now through water 404 (Figs. 3 and 4). Loss of the direct hydrogen bond between Glu^{194} and Glu^{204} in the M state is expected if the source of the released proton is a proton shared between Glu^{194} and Glu^{204} (*3*) or either Glu^{204} or Glu^{194}. Indeed, the positive charge of Arg^{82} is now closer to the two glutamates and would stabilize them if they were both anions after release of the proton to the extracellular surface.

Conformational Changes in the Cytoplasmic Region

Low-resolution (≥3 Å) diffraction difference maps in projection (*8, 14*) and cryoelectron microscopy of tilted samples (*7*) had indicated that large structural changes occur in the cytoplasmic (but not the extracellular) region of the

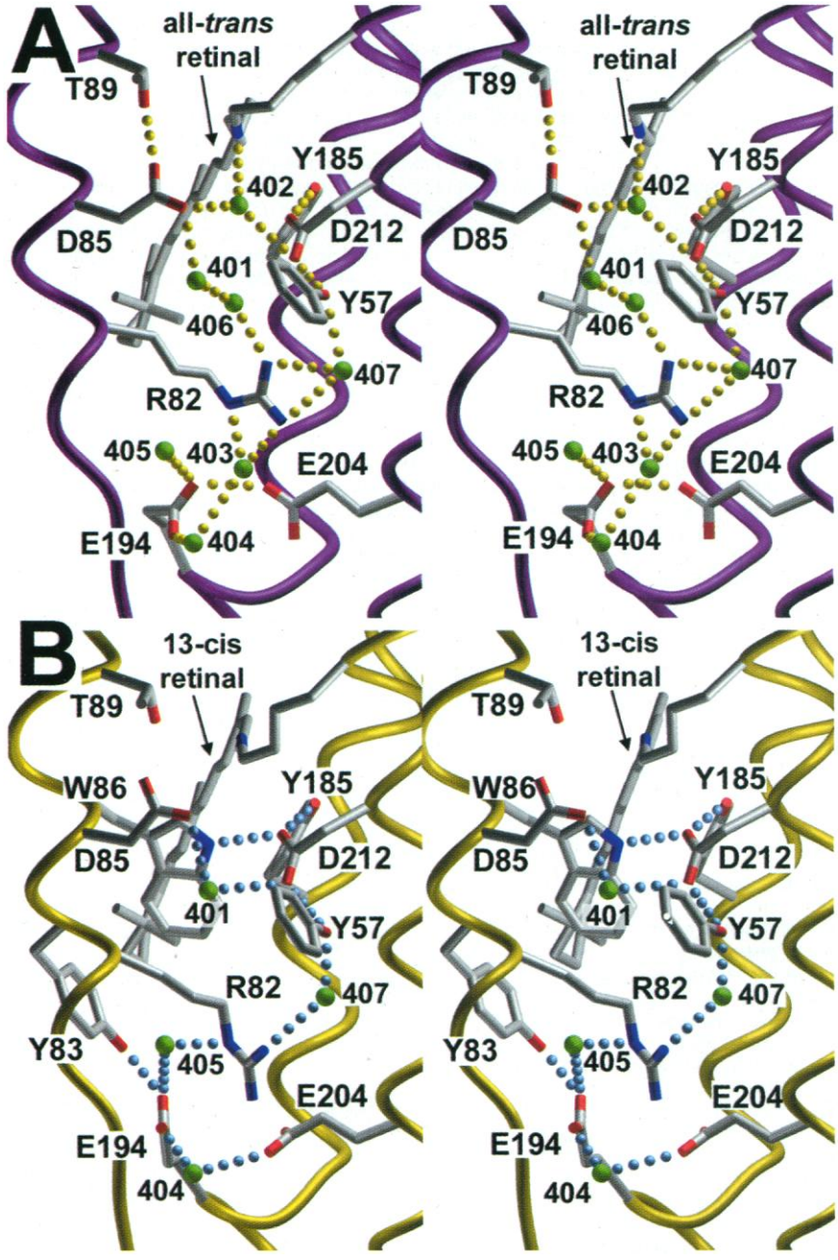

Fig. 3. Stereoviews of the structure and hydrogen bonding of the extracellular region in the BR state **(A)** and the M state **(B)**. The extensive hydrogen-bonding network leading to the extracellular surface found in the BR state is fragmented in the M state. Notable are new hydrogen bonds formed in the M state between Trp^{86} NE and Asp^{212} OD-1 and between Tyr^{83} OH and Glu^{194} OE-1; the carboxylate side chain of Asp^{85} has lost a hydrogen bond from Thr^{89} OH; the guanidinium moiety of Arg^{82} has moved away from the Schiff base and toward the extracellular side (downward) by 1.7 Å, largely because of a rotation around χ_3 by 60°.

protein in the M and N intermediates. The most prominent of these are the tilt of the cytoplasmic end of helix F away from the center of the protein and an increase of density of uncertain origin at helix G. We find that these two helices are strongly and uniquely affected in the M state. From the refined temperature factors of main-chain atoms, it is clear that the cytoplasmic ends of helices F and G are disordered between the E-F interhelical loop and residue 176 and beyond residue 222, respectively (Fig. 5). This is unlike the BR state of D96N, where these regions could be modeled as far to the surface as residues 162 and 231, respectively. In the region where the temperature factors were low enough to allow modeling, notable root-mean-square deviations between the BR and M states of D96N could be seen in helix G but not in helix F, with the exception of the two residues nearest its disordered segment. The movement of the main chain at these two residues is away from the center of the molecule, as concluded previously from projection difference maps (*7, 8, 14*), with the α carbon of the first residue to move, Val^{177}, displaced by 1.6 Å. If there is a tilt in the M state, it can therefore involve only the segment between residues 162 and 177 instead of the entire cytoplasmic half of helix F, with Tyr^{185} and Pro^{186} acting as a hinge, as is often assumed. The position of the ring of Tyr^{185} also remains virtually unchanged in M. No displacements of the main chain are evident in helices A to E.

The main-chain movements within helix G involve the local region around Ala^{215} and Lys^{216}, where the π bulge was described (*6*). The change of the main chain of helix G in the M and BR states is shown in Fig. 6. The peptide of carbonyl 215, which in the BR state is tilted outward and away from the helix axis, is now aligned with the helix axis. In contrast, the peptide of carbonyl 216, which in the BR state accepts a hydrogen bond from amide 220, is now tilted away, resulting in a loss of the α-helical hydrogen bond. These local conformational changes of the π bulge are likely a direct consequence of the strain induced by retinal isomerization.

In the unphotolyzed state of the D96N mutant, there is no hydrogen-bonded network in the cytoplasmic half of the protein comparable to that in the extracellular half, although the main-chain carbonyl groups of Ala^{215} and Lys^{216} are hydrogen-bonded to water molecules 501 and 503 and to water molecules 502 and 504, respectively. Because these features are located where the retinal is bound (to Lys^{216}) and because water molecules 501 and 504 are hydrogen-bonded to the NE of Trp^{182} (a residue in contact with the retinal) and to ND-2 of Asn^{96} (a residue in the proton transfer pathway that leads to the cytoplasmic surface), respectively, they are likely to have functional significance. Indeed, we find that this structure is disrupted in the M state, and no density can be seen for water molecules 501 and 504. The relocation of water 501 must be caused by main-chain and side-chain motions (Figs. 2 and 6) that increase the distance between the O of Ala^{215} and NE of Trp^{182} from 5.4 to 7.6 Å. If there are bound water molecules in the M state in this region, as suggested previously (*28–30*), they are disordered and do not form a hydrogen-bonded network as exists in the extracellular half of the protein. How then is the proton conducted from the cytoplasmic surface to the Schiff base?

The primary barrier to proton conduction in the cytoplasmic region is a constellation of hydrophobic residues that occlude the interhelical cleft (*2–6*). In Fig. 2 the side chains of the most prominent of these, Leu^{93} and Phe^{219}, are seen to rotate away to provide the possibility of a pathway between the surface and the Schiff base. Unlike in the wild type, the very slow

Table 1. X-ray data collection and refinement statistics. Crystals of the D96N mutant of bacteriorhodopsin grown in the cubic lipid phase are isomorphous to wild-type crystals and form thin hexagonal plates, typically about 60 μm by 60 μm by 15 μm with space group $P6_3$ and merohedral twinning (*19*). After mechanical extraction of the crystals, the adhering cubic lipid phase was removed by soaking for several hours in 0.1 % octyl glucoside solution containing 3 M sodium phosphate (pH 5.6). Diffraction data were collected from cryocooled (100 K) crystals at beamline 5.0.2 at the Advanced Light Source (ALS, Berkeley) with a 2 by 2 array charge-coupled device (CCD) detector (ADSC, San Diego) and at the microfocus beamline ID13 at the European Synchrotron Research Facility (ESRF, Grenoble) with a CCD detector (MARResearch, Hamburg). For the BR state structure, a single crystal was light-adapted before cryocooling. For the M state structure, a light-adapted crystal was first cryocooled, and then the cryostream was blocked for 3 s while the crystal was illuminated with yellow light (>520 nm) from a halogen lamp. The crystals became colorless, indicating complete conversion to M with deprotonated Schiff base. Still pictures and a video of the light-induced conversion of a D96N crystal to the M state can be viewed at http://anx12.bio.uci.edu/~hudel/br/m/bleach.html. Diffraction images were integrated, scaled, and merged with DENZO/SCALEPACK (*39*). The starting model 1C3W (*6*) was refined against BR-state structure factors with SHELXL-97 (*40*), taking merohedral twinning into account. The position of the nitrogen of the Asn^{96} side-chain amide was unambiguously determined by inspection of the refined temperature factors for both possible conformations. $F_o - F_c$ maps were used to locate additional water molecules. Subsequently, the refined BR-state D96N structure was refined against four independent sets of M state structure factors. In several cases, 20 cycles of conjugate gradient minimization with SHELXL were sufficient to yield 13-*cis*-retinal without manual refitting. In all cases, the temperature factors for the cytoplasmic ends of helices F and G (residues 162 to 175 and 223 to 231, respectively) refined to values above 60 $Å^2$ (Fig. 5), and the corresponding densities were too poor to allow interpretation. Omit maps and $3F_o - 2F_c$ maps were used extensively in refitting the retinal, side-chain conformations and in locating water molecules. The final M state model includes residues 5 to 156, 176 to 222, the covalently linked 13-*cis*-retinal, 14 water molecules, and 12 lipid molecules.

Data reduction resolution range	BR state		M state	
	1.8–25 Å	1.80–1.83 Å	2.0–25 Å	2.00–2.03 Å
Total observations	167,219		110,517	
Unique structure factors	19,005		14,622	
Mosaicity (°)	0.26		0.81	
Average $I/\sigma(I)$†	24.0	5.4	19.2	2.1
Completeness (%)	88.1	87.5	95.0	98.1
R_{merge}* (%)	5.7	21.6	6.9	33.0
Refinement resolution range		1.8–12		2.0–12 Å
Number of structure factors		18,388		14,622
Number of restraints		8,229		7,361
Number of parameters		8,308		7,292
Twin ratio		53:47		53:47
Number of protein atoms		1,720		1,535
Number of retinal atoms		20		20
Number of water molecules		46		14
Number of lipid atoms		310		277
R factor‡ (%) for data with $F > 4\sigma(F)$/all data		12.1/12.6		17.2/20.6
R_{free}§ (%) for data with $F > 4\sigma(F)$/all data		17.9/18.2		21.9/25.5
Average protein B ($Å^2$)		26.6		33.1
Average retinal B ($Å^2$)		20.0		26.8
Average water B ($Å^2$)		33.0		44.7
Average lipid B ($Å^2$)		52.8		48.9
Deviation from ideal bond lengths (Å)		0.009		0.007
Deviation from ideal bond angle distances (Å)		0.025		0.021

*$R_{merge}(I) = \Sigma_{hkl}\Sigma_i |I_{hkl,i} - \langle I_{hkl}\rangle| / \Sigma_{hkl}\Sigma_i |I_{hkl,i}|$, where $\langle I_{hkl}\rangle$ is the average intensity of the multiple $I_{hkl,i}$ observations for symmetry-related reflections. †$I/\sigma(I)$, average of the diffraction intensities, divided by their standard deviations. ‡R factor $= \Sigma_{hkl}||F_o| - |F_c|| / \Sigma_{hkl}|F_o|$, where F_o and F_c are observed and calculated structure factors, respectively. §$R_{free} = \Sigma_{hkl \in T}||F_o| - |F_c|| / \Sigma_{hkl \in T}|F_o|$, where the test set (5% of the data) is omitted from the refinement in such a way that all structure factors in each of several thin resolution shells were selected to avoid bias due to the presence of merohedral twinning.

decay of the M state of the D96N mutant (at pH 7, τ = tens of seconds) is limited by proton uptake at the surface (*29, 31*), and its greatly increased entropic barrier was suggested to reflect a structural requirement for capturing the proton from the bulk (*29*). Presumably, M decay occurs when either hydrogen-bonding groups (of necessity, water molecules) form a transient proton-conducting network from the surface to the Schiff base or mobile water molecule(s) carry a proton through a transiently opened tortuous pathway. This structural transition will not yet have taken place in M_N, although the disorder of the cytoplasmic ends of helices F and G hint at conformational changes that make the region above Asn^{96} more permeable to water.

Structural Clues to the Mechanism of Proton Transport

The structure of the M state at 2 Å resolution reveals clear changes at the retinal and in the extracellular region that occur after isomerization, proton transfer to Asp^{85} and proton release, and less well defined changes in the cytoplasmic region that prepare it for proton uptake in the M-to-N step. What do these changes tell about the way the excess free energy acquired by photoisomerization of the retinal is used to generate an electrochemical gradient for protons across the membrane? Initially, the free energy gain must be localized in a steric and electrostatic conflict between the retinal and its binding site. In the M state, four hydrogen bonds at the immediate active site are broken (Fig. 4), and the side chains of Trp^{86}, Trp^{182}, and Leu^{93} are displaced (Fig. 2) to accommodate the upward movement of the 13-methyl group of the retinal. However, we had found (*32*) that full relaxation of the binding site, so as to favor the 13-*cis*,15-*anti* form at the expense of the all-*trans* form, is realized only after both protonation of Asp^{85} and deprotonation of the Schiff base (that is, proton transfer toward the extracellular side) and deprotonation of Asp^{96} and reprotonation of the Schiff base (that is, proton transfer from the cytoplasmic side). The central question then is: What determines the direction of these proton movements to and from the Schiff base—that is, what is the nature of the protonation switch?

In principle, the switch may reside in either the retinal or the protein, possibilities that are not necessarily mutually exclusive. Examples for the first include a proposed rotation around the C-14–C-15 single bond of the retinal that would reorient the retinylidene nitrogen after its deprotonation but before its reprotonation (*33*), and a proposed change of the curvature of the polyene chain upon deprotonation of the Schiff base that would move the retinylidene nitrogen toward the cytoplasmic side to connect with a proton conducting channel (*14*). Studies of the photocycle of the D85N–D96N mutant (*34*) suggested that, in this case at least, once the retinal is isomerized to 13-*cis*,15-*anti* the active site allows access to both directions (local access), and the direction of proton movement is determined by the changing proton conductivities in the extracellular and cytoplasmic half-channels. If this mechanism is relevant to the function of wild-type bacteriorhodopsin as proposed (*34*), then for directional transport the proton-transfer pathways to and from the Schiff base must be made and broken in a timely manner.

The configurational changes of the retinal in the M state do not support the idea of rotation of the C-14–C-15 bond. Although the Schiff base nitrogen is displaced toward the cytoplasmic direction and now faces away from Asp^{85} (Figs. 2 to 4), it seems more likely that this occurs as the result of the isomerization to 13-*cis*,15-*anti* instead of deprotonation of the retinylidene nitrogen. If this were indeed so, it would exclude the Schiff base as the crucial element of the accessibility switch. It is not yet clear, in any case, how the proton is transferred to and from the Schiff base. On the other hand, the structure of the M state reveals that the protein does participate in the switch reaction. There are structural changes in the extracellular region (Figs. 3 and 4) that include displacement of the Arg^{82} side chain away from the active site and the loss of critical water molecules, changes that affect the proton affinity of Asp^{85}. From the pH dependencies of the kinetics of the M_1-to-M_2 transition, it appeared that the protonation equilibrium that develops between the Schiff base and Asp^{85} in the early M state shifts to full proton transfer in the late M state upon release of a proton to the extracellular surface (*13*). This would occur through the observed coupling of the protonation states of Asp^{85} and the proton release site (*26*). The first increase in the pK_a of Asp^{85} that leads to the L ↔ M_1 equilibrium (*13, 26, 27*) must originate from disruption of the hydrogen bonds that the an-

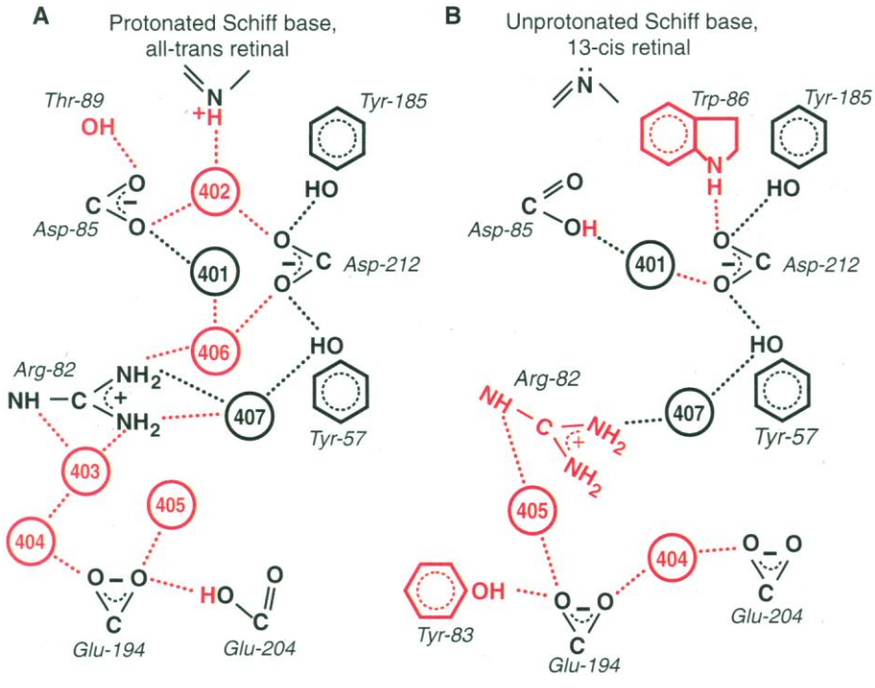

Fig. 4. Schematic representation of hydrogen bonds between side-chain groups and bound water in the extracellular region in the BR state (**A**) and the M state (**B**). Water molecules, protons, and hydrogen bonds in the BR state that undergo change are shown in red. Water molecules, hydrogen bonds, and residue side chains in the M state that are different or moved from the BR state are also red. Glu^{194} and Glu^{204} are both shown as anionic in M, although time-resolved FTIR spectra do not contain the expected negative C=O stretch band (*38*).

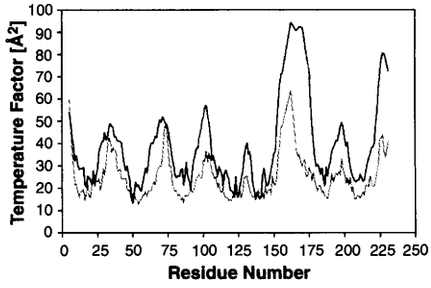

Fig. 5. Conformational changes of the main chain in the M state. Refined temperature factors for main-chain atoms in the BR state (gray) and the M state (black). Regions of high temperature factors are usually found at the NH_2- and COOH-termini, as well as in the loops on the extracellular and cytoplasmic faces. The regions between residues 162 and 175, as well as between residues 223 and 231, have significantly higher temperature factors in the M state, are highly disordered, and have been omitted from the final model (Table 1).

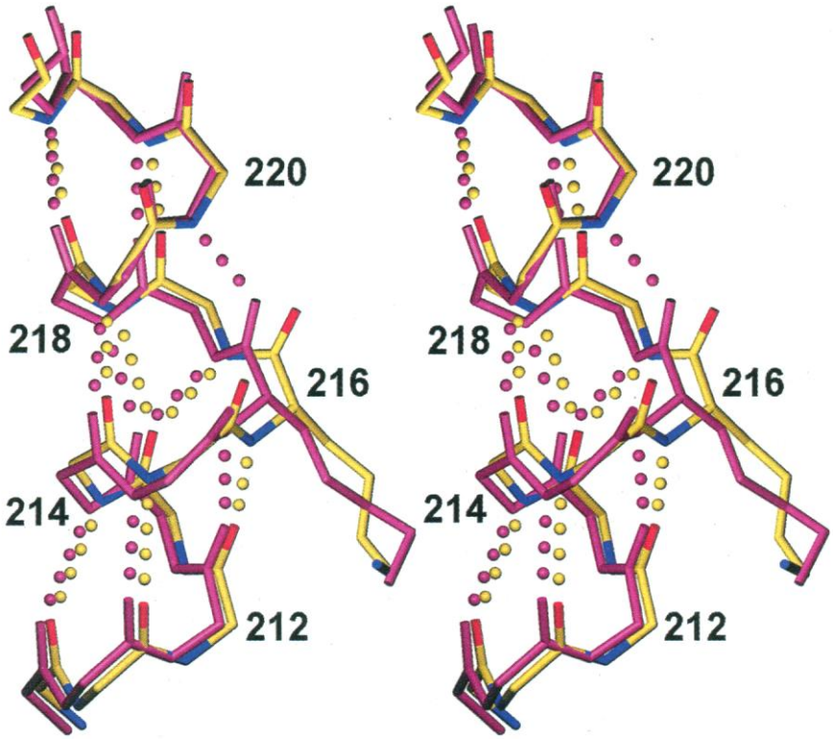

Fig. 6. Stereo view of the conformational change of helix G in the M state at Ala^{215}-Lys^{216}. Residues 210 to 222 of helix G are shown, with the BR state in purple and the M state in yellow. In the BR state, the peptide of carbonyl 215 is tilted outward and away from the helix axis, and it is connected to Trp^{182} NE via water 501. In the M state, the peptide is realigned with the helix axis. In contrast, the peptide of carbonyl 216, which in the BR state is accepting a hydrogen bond from amide 220, is now tilted away from the helix axis, resulting in a loss of the interhelical hydrogen bond due to an increase in the distance between main-chain 220 N and main-chain 216 O from 2.9 to 4.2 Å. The α carbon of Lys^{216} moves 1.0 Å toward the extracellular side, presumably because of strain induced after isomerization of the covalently attached retinal.

ionic Asp^{85} received from water 402 and Thr^{89}, and the loss of several water molecules. A second increase, which leads to transition to the late M state, is provided by the movement of the side chain of Arg^{82} away from Asp^{85} upon proton release (Figs. 3 and 4). Thus, it appears that shuttling of the positive charge of Arg^{82} between an inward and an outward direction (*35*) is what mediates the coupling between the protonation states of Asp^{85} and the proton release site. After proton release, its high pK_a keeps Asp^{85} protonated, and this ensures that reprotonation of the Schiff base is from the cytoplasmic side.

In the BR state the cytoplasmic region does not contain an interconnected hydrogen-bonded network, as expected because bacteriorhodopsin does not conduct protons passively. The most severe structural changes during the photocycle are in the cytoplasmic portions of helices F and G (*7, 14*). In M_N these conformational changes cannot be far from the cytoplasmic surface, because we observe no significant rigid-body displacements of helices F and G, to within 12 and 3 residues, respectively, from the helical ends in the BR state (Fig. 5). We detect this kind of structural change in helices F and G only as the severe disordering of regions that are ordered in the BR state instead of as a discrete conformational state. A relationship of the tilt of helix F to proton uptake at the cytoplasmic surface had been implied by the alterations of the photocycle kinetics when bulky groups were introduced into this region or helix F was cross-linked (*36*). We observe an additional and unusual conformational change near the bilayer center for helix G, at the π bulge (Fig. 6). It may be because of this change of helix G and residues in the retinal binding site, and the resulting displacements of side chains and bound water, that a transient proton-conduction pathway forms that allows reprotonation of the Schiff base, but the structure of M provides only hints about how this could happen.

References and Notes

1. J. K. Lanyi, *J. Struct. Biol.* **124**, 164 (1998); U. Haupts, J. Tittor, D. Oesterhelt, *Annu. Rev. Biophys. Biomol. Struct.* **28**, 367 (1999).
2. E. Pebay-Peyroula, G. Rummel, J. P. Rosenbusch, E. M. Landau, *Science* **277**, 1676 (1997); H. Belrhani *et al.*, *Structure* **7**, 909 (1999).
3. L. O. Essen, R. Siegert, W. D. Lehmann, D. Oesterhelt, *Proc. Natl. Acad. Sci. U.S.A.* **95**, 11673 (1998).
4. H. Luecke, H. T. Richter, J. K. Lanyi, *Science* **280**, 1934 (1998).
5. Y. Kimura *et al.*, *Nature* **389**, 206 (1997); N. Grigorieff, T. A. Ceska, K. H. Downing, J. M. Baldwin, R. Henderson, *J. Mol. Biol.* **259**, 393 (1996).
6. H. Luecke, B. Schobert, H. T. Richter, J.-P. Cartailler, J. K. Lanyi, *J. Mol. Biol.* **291**, 899 (1999).
7. S. Subramaniam, M. Gerstein, D. Oesterhelt, R. Henderson, *EMBO J.* **12**, 1 (1993); J. Vonck, *Biochemistry* **35**, 5870 (1996).
8. H. Kamikubo *et al.*, *Proc. Natl. Acad. Sci. U.S.A.* **93**, 1386 (1996).
9. J. K. Lanyi and G. Váró, *Israel J. Chem.* **35**, 365 (1995).
10. S. Dickopf and M. P. Heyn, *Biophys. J.* **73**, 3171 (1997); G. Nagel, B. Kelety, B. Möckel, G. Büldt, E. Bamberg, *ibid.* **74**, 403 (1998).
11. L. S. Brown, A. K. Dioumaev, R. Needleman, J. K. Lanyi, *ibid.* **75**, 1455 (1998).
12. G. Váró and J. K. Lanyi, *Biochemistry* **30**, 5016 (1991).
13. L. Zimányi *et al.*, *ibid.* **31**, 8535 (1992).
14. S. Subramaniam *et al.*, *J. Mol. Biol.* **287**, 145 (1999).
15. M. S. Braiman, O. Bousché, K. J. Rothschild, *Proc. Natl. Acad. Sci. U.S.A.* **88**, 2388 (1991); B. Hessling, G. Souvignier, K. Gerwert, *Biophys. J.* **65**, 1929 (1993).
16. T. E. Thorgeirsson *et al.*, *J. Mol. Biol.* **273**, 951 (1997).
17. J. Sasaki, Y. Shichida, J. K. Lanyi, A. Maeda, *J. Biol. Chem.* **267**, 20782 (1992).
18. C. Rödig and F. Siebert, *FEBS Lett.* **445**, 14 (1999).
19. G. Rummel *et al.*, *J. Struct. Biol.* **121**, 82 (1998).
20. M. Kataoka *et al.*, *J. Mol. Biol.* **243**, 621 (1994).
21. B. Borucki, H. Otto, M. P. Heyn, *J. Phys. Chem. B* **102**, 3821 (1998); T. N. Earnest, P. Roepe, M. S. Braiman, J. Gillespie, K. J. Rothschild, *Biochemistry* **25**, 7793 (1986).
22. S. Moltke *et al.*, *Biochemistry* **37**, 11821 (1998).
23. S. Subramaniam, D. A. Greenhalgh, P. Rath, K. J. Rothschild, H. G. Khorana, *Proc. Natl. Acad. Sci. U.S.A.* **88**, 6873 (1991); H. Kandori *et al.*, *Biochemistry* **36**, 5134 (1997).
24. O. Weidlich *et al.*, *Biochemistry* **35**, 10807 (1996).
25. L. S. Brown and J. K. Lanyi, *Proc. Natl. Acad. Sci. U.S.A.* **93**, 1731 (1996).
26. S. P. Balashov, E. S. Imasheva, R. Govindjee, T. G. Ebrey, *Biophys. J.* **70**, 473 (1996); H.-T. Richter, L. S. Brown, R. Needleman, J. K. Lanyi, *Biochemistry* **35**, 4054 (1996).
27. M. S. Braiman, A. K. Dioumaev, J. R. Lewis, *Biophys. J.* **70**, 939 (1996).
28. G. Váró and J. K. Lanyi, *ibid.* **59**, 313 (1991).
29. Y. Cao *et al.*, *Biochemistry* **30**, 10972 (1991).
30. H.J. Sass *et al.*, *EMBO J.* **16**, 1484 (1997); H. Kamikubo *et al.*, *Biochemistry* **36**, 12282 (1997).
31. M. Holz *et al.*, *Proc. Natl. Acad. Sci. U.S.A.* **86**, 2167 (1989); J. Tittor, C. Soell, D. Oesterhelt, H.-J. Butt, E. Bamberg, *EMBO J.* **8**, 3477 (1989).
32. A. K. Dioumaev, L. S. Brown, R. Needleman, J. K. Lanyi, *Biochemistry* **37**, 9889 (1998).
33. K. Schulten and P. Tavan, *Nature* **272**, 85 (1978); D. Oesterhelt, P. Hegemann, P. Tavan, K. Schulten, *Eur. Biophys. J.* **14**, 123 (1986); K. Gerwert and F. Siebert, *EMBO J.* **5**, 805 (1986).
34. L. S. Brown, A. K. Dioumaev, R. Needleman, J. K. Lanyi, *Biochemistry* **37**, 3982 (1998).
35. C. Scharnagl, J. Hettenkofer, S. F. Fischer, *J. Phys. Chem.* **99**, 7787 (1995).
36. L. S. Brown, G. Váró, R. Needleman, J. K. Lanyi, *Biophys. J.* **69**, 2103 (1995).
37. Abbreviations for amino acid residues are as follows: A, Ala; C, Cys; D, Asp; E, Glu; F, Phe; G. Gly; H, His; I, Ile; K, Lys; L, Leu; M, Met; N, Asn; P, Pro; Q, Gln; R, Arg; S, Ser; T, Thr; V, Val; W, Trp; and Y, Tyr.
38. R. Rammelsberg, G. Huhn, M. Lübben, K. Gerwert, *Biochemistry* **37**, 5001 (1998).
39. Z. Otwinowski, in *Data Collection and Processing*, L. Sawyer, N. Isaacs, S. Bailey, Eds. (SERC Daresbury Laboratory, Warrington, U.K., 1993), p. 56.
40. G. M. Sheldrick and T. Schneider, *Methods Enzymol.* **277**, 319 (1997).

41. Supported in part by grants from the National Institutes of Health to H.L. (R01-GM56445 and R01-GM59970) and J.K.L. (R01-GM29498) and from the Department of Energy to J.K.L. (DEFG03-86ER13525). The atomic coordinates of the BR and M states of the D96N mutant of bacteriorhodopsin have been deposited in the Protein Data Bank (accession numbers 1C8R and 1C8S, respectively).

28 June 1999; accepted 2 August 1999

References and Notes

[2] **X-ray Structure of Bacteriorhodopsin at 2.5 Angstroms from Microcrystals Grown in Lipidic Cubic Phases**

Eva Pebay-Peyroula; Gabriele Rummel; Jurg P. Rosenbusch; Ehud M. Landau

Science, New Series, Vol. 277, No. 5332. (Sep. 12, 1997), pp. 1676-1681.

Stable URL:

http://links.jstor.org/sici?sici=0036-8075%2819970912%293%3A277%3A5332%3C1676%3AXSOBA2%3E2.0.CO%3B2-F

[3] **Lipid Patches in Membrane Protein Oligomers: Crystal Structure of the Bacteriorhodopsin-Lipid Complex**

L.-O. Essen; R. Siegert; W. D. Lehmann; D. Oesterhelt

Proceedings of the National Academy of Sciences of the United States of America, Vol. 95, No. 20. (Sep. 29, 1998), pp. 11673-11678.

Stable URL:

http://links.jstor.org/sici?sici=0027-8424%2819980929%2995%3A20%3C11673%3ALPIMPO%3E2.0.CO%3B2-E

[4] **Proton Transfer Pathways in Bacteriorhodopsin at 2.3 Angstrom Resolution**

Hartmut Luecke; Hans-Thomas Richter; Janos K. Lanyi

Science, New Series, Vol. 280, No. 5371. (Jun. 19, 1998), pp. 1934-1937.

Stable URL:

http://links.jstor.org/sici?sici=0036-8075%2819980619%293%3A280%3A5371%3C1934%3APTPIBA%3E2.0.CO%3B2-J

LINKED CITATIONS

[8] **Structure of the N Intermediate of Bacteriorhodopsin Revealed by X-Ray Diffraction**

Hironari Kamikubo; Mikio Kataoka; Gyorgy Varo; Toshihiko Oka; Fumio Tokunaga; Richard Needleman; Janos K. Lanyi

Proceedings of the National Academy of Sciences of the United States of America, Vol. 93, No. 4. (Feb. 20, 1996), pp. 1386-1390.

Stable URL:

http://links.jstor.org/sici?sici=0027-8424%2819960220%2993%3A4%3C1386%3ASOTNIO%3E2.0.CO%3B2-H

[15] **Protein Dynamics in the Bacteriorhodopsin Photocycle: Submillisecond Fourier Transform Infrared Spectra of the L, M, and N Photointermediates**

Mark S. Braiman; Olaf Bousche; Kenneth J. Rothschild

Proceedings of the National Academy of Sciences of the United States of America, Vol. 88, No. 6. (Mar. 15, 1991), pp. 2388-2392.

Stable URL:

http://links.jstor.org/sici?sici=0027-8424%2819910315%2988%3A6%3C2388%3APDITBP%3E2.0.CO%3B2-R

[23] **Replacement of Leucine-93 by Alanine or Threonine Slows Down the Decay of the N and O Intermediates in the Photocycle of Bacteriorhodopsin: Implications for Proton Uptake and 13-cis-Retinal → all-Trans-Retinal Reisomerization**

Sriram Subramaniam; Duncan A. Greenhalgh; Parshuram Rath; Kenneth J. Rothschild; H. Gobind Khorana

Proceedings of the National Academy of Sciences of the United States of America, Vol. 88, No. 15. (Aug. 1, 1991), pp. 6873-6877.

Stable URL:

http://links.jstor.org/sici?sici=0027-8424%2819910801%2988%3A15%3C6873%3AROLBAO%3E2.0.CO%3B2-A

[25] **Determination of the Transiently Lowered pK _a of the Retinal Schiff Base during the Photocycle of Bacteriorhodopsin**

Leonid S. Brown; Janos K. Lanyi

Proceedings of the National Academy of Sciences of the United States of America, Vol. 93, No. 4. (Feb. 20, 1996), pp. 1731-1734.

Stable URL:

http://links.jstor.org/sici?sici=0027-8424%2819960220%2993%3A4%3C1731%3ADOTTLP%3E2.0.CO%3B2-O

LINKED CITATIONS

[31] **Replacement of Aspartic Acid-96 by Asparagine in Bacteriorhodopsin Slows Both the Decay of the M Intermediate and the Associated Proton Movement**

Martin Holz; Lel A. Drachev; Tatsushi Mogi; Harald Otto; Andrey D. Kaulen; Maarten P. Heyn; Vladimir P. Skulachev; H. Gobind Khorana

Proceedings of the National Academy of Sciences of the United States of America, Vol. 86, No. 7. (Apr. 1, 1989), pp. 2167-2171.

Stable URL:

http://links.jstor.org/sici?sici=0027-8424%2819890401%2986%3A7%3C2167%3AROAABA%3E2.0.CO%3B2-4